Phenotype-based screens with conformation-specific inhibitors reveal p38 gamma and delta as targets for HCC polypharmacology

Jia Xin Yu*[1,2,4], Amanda J. Craig*[3,4], Mary E. Duffy*[1,2,4], Carlos Villacorta-Martin[3], Verónica Miguela[1,3,5], Marina Ruiz de Galarreta[1,3,5], Alexander P. Scopton[1,2], Lisa Silber[1,2], Andres Y. Maldonado[1,2], Alexander Rialdi[1,3,4], Ernesto Guccione[1,3,4], Amaia Lujambio[1,3,4,5], Augusto Villanueva[3,4,6], Arvin C. Dar[1,2,4]

Affiliations:

[1]Department of Oncological Sciences, The Tisch Cancer Institute, The Icahn School of Medicine at Mount Sinai, New York, New York 10029, USA

[2]Department of Pharmacological Sciences, The Tisch Cancer Institute, The Icahn School of Medicine at Mount Sinai, New York, New York 10029, USA

[3]Liver Cancer Program, Division of Liver Diseases, Department of Medicine, Tisch Cancer Institute, Icahn School of Medicine at Mount Sinai, New York, USA

[4]Graduate School of Biomedical Sciences at Icahn School of Medicine at Mount Sinai, New York, USA

[5]Precision Immunology Institute at Icahn School of Medicine at Mount Sinai, New York, USA

[6]Division of Hematology and Medical Oncology, Department of Medicine, Icahn School of Medicine at Mount Sinai, New York, New York, USA.

*Co-first authors

Running Title: p38 delta and gamma as targets for HCC polypharmacology

Corresponding authors.

Arvin Dar (arvin.dar@mssm.edu; 212-824-8863; 1470 Madison Avenue, S6-105, NYC, NY, 10029), Augusto Villanueva (augusto.villanueva@mssm.edu; 212-659-9392; 1425 Madison Ave, RM 11-70E, Box 1123, NYC, NY, 10029); and Amaia Lujambio (amaia.lujambio@mssm.edu; 212-824-9338; 1470 Madison Avenue, S6-111, NYC, NY, 10029).

Conflicts of Interest: AV has received consulting fees from Guidepoint and Fujifilm; advisory board fees from Exact Sciences and Nucleix; and lecture fees from Exelixis. Mount Sinai holds a joint patent on AD80 (W0/2013/077921).

ABSTRACT:

The approved kinase inhibitors for hepatocellular carcinoma (HCC) are not matched to specific mutations within tumors. This has presented a daunting challenge; without a clear target or mechanism, no straightforward path has existed to guide the development of improved therapies for HCC. Here we combine phenotypic screens with a class of conformation-specific kinase inhibitors termed type II to identify a multi-kinase inhibitor - AD80 - with anti-tumoral activity across a variety of HCC preclinical models, including mouse xenografts. Mass spectrometry profiling found a number of kinases as putative targets for AD80, including several receptor and cytoplasmic protein kinases. Among these, we found p38 gamma and delta as direct targets of AD80. Notably, a closely related analog of AD80 lacking p38δ/γ activity, but retaining several other off-target kinases, lost significant activity in several HCC models. Moreover, forced and sustained MKK6➔p38➔ATF2 signaling led to a significant reduction of AD80 activity within HCC cell lines. Together with HCC survival data in The Cancer Genome Atlas (TCGA) and RNA-seq analysis, we suggest p38 delta and gamma as therapeutic targets in HCC and an "AD80 inhibition signature" as identifying those patients with best clinical outcomes.

INTRODUCTION:

Liver cancer is the fourth greatest cause of cancer related mortality, accounting for nearly 800,000 annual deaths(1). The mortality rates for hepatocellular carcinoma (HCC), which makes up to 70-85% of liver cancer cases, have been rising dramatically(2). Based on data between 1995 and 2009 in the US, liver cancer (including HCC and intrahepatic cholangiocarcinoma) mortality rates increased 41.2% and 62.8% for females and males, respectively(3).

Liver cancer presents several unique challenges for the identification of drug targets and therapeutics. For example, the most frequent mutations in HCC patients (i.e., *TERT* promoter, *TP53* and *CTNNB1*) are broadly considered undruggable(2). Additionally, there are on average 2.5 genetic aberrations per Mb in HCC patients(4–6), with significant variation either between or within tumors(7). As such, clear and actionable driver mutations analogous to the $BRAF^{V600E}$ allele in melanoma have not yet been found(4,8). Moreover, individuals with HCC often suffer from cirrhosis; a further complication that can enhance the apparent liver toxicity of drugs and thereby narrow the therapeutic index (e.g. sunitinib(9)).

Clinical studies have revealed advanced stage HCC patients as particularly sensitive to kinase inhibitors (KIs), including the first approved therapy for HCC sorafenib(10), and more recently lenvatinib(11), cabozantinib(12), and regorafenib(13). While highly encouraging, a 5-year survival rate of only 18% in these patients highlights a need to further improve upon current therapies.

Critical targets for sorafenib include kinases within tumor cells (e.g. RAF1) and the microenvironment (VEGFR1)(14); however, the exact mechanism for how this drug operates remains controversial. Recent work has suggested that additional kinases, including p38α/MAPK14(15) and Aurora A(16), may be targeted to increase the efficacy of sorafenib and reduce susceptibility to emergent resistance. Clearly, multi-targeted kinase inhibitor activity for HCC has proven successful; however, identifying optimal targets and mode of modulation to improve upon current therapies remains challenging.

Sorafenib and regorafenib belong to a subclass of KIs termed type II inhibitors. These compounds, along with cabozantinib and lenvatinib, share several related structural motifs, including a hinge-binding element, linker, and cap (**Fig. 1A**). The linker

and cap motifs in particular are critical for conformationally-selective target engagement. Unlike type I compounds, which bind to the DFG (aspartate-phenylalanine-glycine)-in (**Fig. 1B**) conformation of active state kinases, type II compounds require an inactive state configuration characterized by a flip of the conserved DFG tripeptide within the kinase active site to enable drug binding (**Fig. 1C**). Within the active state, the type II pocket is occluded through direct contacts to Mg and ATP. While the mode of engagement by sorafenib, regorafenib, cabozantinib, and lenvatinib(17) is similar, the precise kinase targets for these compounds vary(14,18) and likely contribute to the differing biological efficacy for each drug.

Recognizing the high activity of the above-mentioned KIs in HCC, which may depend on both (i) specific target profiles and (ii) mode of inhibition, we speculated that there might exist additional unidentified kinase dependencies for targeting HCC that may be revealed via conformation-specific inhibition. We therefore screened a focused library of type II KIs within preclinical models of HCC with the purpose of identifying kinase profiles and companion inhibitors that would improve upon current therapies. These studies identified a class of type II KIs with broad polypharmacology yet pronounced selectivity for tumor over normal cells. Further, we identified the kinases p38 gamma and delta as therapeutic targets for HCC.

MATERIALS AND METHODS:

Cell Culture

HUH7, SNU398, LI-7, HEP3B, THLE5B, and PLC/PRF/5 cells were authenticated by short tandem repeat profiling. THLE5B cells were provided by the Yujin Hoshida Lab at the Icahn School of Medicine at Mount Sinai. All lines tested negative for mycoplasma contamination. HUH7, SNU398, HEP3B, and PLC/PRF/5 cells were maintained in DMEM with 10% fetal bovine serum (FBS) supplemented with penicillin/streptomycin. LI-7 cells were maintained in RPMI with 10% FBS supplemented with penicillin/streptomycin. THLE5B cells were maintained in DMEM/F12 with 10% FBS supplemented with penicillin/streptomycin.

Growth Inhibition assays

Growth inhibition assays were performed in 96-well tissue culture treated plates. Specifically, HUH7, SNU398, LI-7, HEP3B, and PLC/PRF/5 cells were plated at 2500 cells per well and treated a day later with inhibitors for 72 hours before measuring growth inhibition. THLE5B were assayed identically except cells were plated at 5000 cells per well. Inhibitor doses ranged from zero (DMSO only) to 20 μM with 0.1% DMSO. Growth inhibition was calculated using fluorescence after applying redox indicator resazurin at 0.05 mg/mL within complete media. Percent growth inhibition was determined by normalizing inhibitor-treated samples to DMSO controls. GI_{50} values were calculated using Prism 7 software (GraphPad Software).

Clonogenic Assays

Clonogenic assays were performed in 100 mm^2 tissue culture treated plates. For HUH7, LI-7, HEP3B, and PLC/PRF/5 cells were plated at ten thousand cells per 100 mm^2 tissue culture treated plates, with inhibitors added after 24 hours. After 14 days of incubation, plates were aspirated, washed with cold PBS, and fixed with cold methanol. Then they were stained with 0.5% crystal violet solution in 25% methanol for 10 minutes and washed with water. All plates were air-dried overnight before scanning at 300 dpi.

Mouse Pharmacokinetic (PK) and Maximum Tolerated Dose (MTD) Studies

For PK, 24 male 6-8-week-old C57Bl6 mice were given 20 mg/kg AD80 in 12.5% KolliphorEl, 12.5% ethanol, and 75% water via oral gavage. Quantities of AD80 in blood plasma were determined by LC-MS/MS at Shanghai Medicilon, Inc. For MTD, five female 6-8-week old C57Bl6 mice were dosed with increasing amounts of AD80 and monitored until minimal clinical signs of toxicity were observed, including but not limited to: lethargy, neurological symptoms, diarrhea, discharges, morbidity, and any other abnormal indication. Body weights were also measured with dose escalations as follows: day 0: 0.1 mg/kg, day 2: 0.2 mg/kg, day 7: 1 mg/kg, day 9: 5 mg/kg, day 14:10 mg/kg, day 16: 20 mg/kg, day 22: 30 mg/kg, day 24: 40 mg/kg, and day 35: 80 mg/kg. All dosing was done using oral gavage in vehicle of 12.5% KolliphorEl, 12.5% ethanol, and 75% water. No signs of toxicity were observed immediately after dosing, except after 80 mg/kg, where one animal displayed hunched posture. MTD for AD80 was determined to be 40 mg/kg.

Xenograft mouse work

Age matched (7-8 weeks) female athymic nude *Foxa1/nu* mice were obtained from Envigo. Prior to injection, HUH7 cells were trypsinized, washed, and resuspended in Gibco Hanks' Balanced Salt Solution without $CaCl_2$, $MgCl_2$,and $MgSO_4$. This suspension was left on ice until injection. Each mouse was injected subcutaneously with 200 µL containing $5x10^6$ HUH7 cells using a 1 mL syringe and 26-gauge needle in the right flank. Post injection, mice were monitored daily for changes in tumor volume at the injection site, by measuring the length and width of the xenograft using a digital caliper and using the simplified equation: $Tumor\ Volume = \frac{1}{2} \times lw^2$ (l, length; w, width). Body weight was assessed three days per week and body condition monitored daily. Inhibitors were dissolved in vehicle of the composition: 1-part Kolliphor El (C5135 from Sigma Aldrich), 1-part ethanol (Sigma Aldrich), and 6-parts 0.22 µm filtered water. When tumors reached a size of ~100 mm^3, animals were allocated for the experiment into three arms: vehicle, sorafenib, and AD80. Animals were dosed once a day every weekday via oral gavage. The tumor growth rate per day per animal was determined using the equation: $\%Tumor\ Growth\ Rate\ Per\ Day = \frac{100\%}{\#Days\ of\ Treatment} \times \frac{(Volume_{Final} - Volume_{Initial})}{Volume_{Initial}}$. Animals

were sacrificed upon reaching 1000 mm^3 or if projected to surpass 1000 mm^3 the following day or weekend. Since each tumor reached endpoint at different times, we used tumor growth to minimize confounding effects from the time course of the experiment. All protocols were approved by IACUC at Icahn School of Medicine at Mount Sinai (2014-0229).

Sample Preparation for SDS-PAGE, Coomassie, and Western Blotting

Cell culture experiments or xenograft samples were harvested and lysed in RIPA buffer with 1X Halt Protease and Phosphatase inhibitor cocktail (Thermo Scientific #78442). Lysates were loaded after dilution with 6X SDS Dye onto Bio-Rad 4–15% Criterion™ Tris-HCl Protein Gel (#3450029). Protein purification samples were diluted with 6X SDS Dye in purification buffers before loading onto Criterion gels.

Gels meant for Coomassie staining were washed with deionized water for 10 minutes, then incubated with 10-20 mL of Bio-Safe Coomassie Stain (item # 1610787) for 30 minutes to 1 hour. Gels were washed with deionized water and de-stained overnight in deionized water. After de-staining, gels were scanned using a flatbed scanner.

Gels meant for subsequent western analysis, were blotted using GE Healthcare Amersham™ Protran™ NC Nitrocellulose Membranes (#45004002). All blots were incubated with primary antibody (1:5000) in 5% bovine serum albumin in TBST. All blots were incubated with secondary antibody (1:5000) in 5% non-fat milk in TBST. Antibodies were obtained from Cell Signaling Technologies: β-Actin (8H10D10) Mouse mAb #3700, Anti-rabbit IgG, HRP-linked Antibody #7074, Anti-mouse IgG, HRP-linked Antibody #7076, Phospho-p44/42 MAPK (Erk1/2) (Thr202/Tyr204) Antibody #9101, Phospho-S6 Ribosomal Protein (Ser235/236) (D57.2.2E) XP® Rabbit mAb #4858, B-Raf (55C6) Rabbit mAb #9433, S6 Ribosomal Protein (5G10) Rabbit mAb #2217, p44/42 MAPK (Erk1/2) (137F5) Rabbit mAb #4695, and c-Myc Antibody #9402.

KiNativ Kinase Profiling

HUH7 cells were cultured, pelleted, and lysed by KiNativ for a final concentration between 5 and 10 mg/mL, from a 1 mL cell pellet. Lysates were split into untreated controls and 1 μM AD80 treatment. After pre-incubation for 10 minutes, the lysates were labeled with

ATP-desthiobiotin and then digested with trypsin. Biotinylated fragments were then enriched via streptavidin pulldown. The samples were subsequently analyzed on Thermo LTQ ion trap mass spectrometers coupled with Agilent 1100 series micro-HPLC systems with autosamplers as described previously by Patricelli et al(19). Treated samples were analyzed in duplicate and untreated samples were run in quadruplicate. Results of kinases profiled with 1 μM and values are shown in Supplemental Table 2.

Expression and Purification

Plasmid-containing HIS-tagged versions of each p38 isoform were synthesized by ATUM (www.atum.bio). Each isoform was expressed in BL21-DE3 cells for growth and expression in terrific broth with kanamycin. The bacteria were cultured at 37˚C with rotation until the optical density reached 0.6, upon which 1 mM IPTG was added to induce protein expression. Bacterial cultures were grown for an additional 16 hours at 18˚C after induction, and then harvested at 4000G for 20 minutes to pellet bacteria. Pellets were re-suspended with cold lysis buffer (25 mM Tris pH 7.5, 10% Glycerol, 150 mM NaCl, 10 mM Imidazole) in the presence of protease inhibitor tablets (Thermo Scientific™ Pierce™ Protease Inhibitor Item# 88666). Bacteria were then lysed on ice, with pulsing sonication. Post sonication, lysates were spun down at 18000G for 20 min to clear the lysate. Cleared lysates were then batch bound onto cobalt-agarose beads (Gold Bio H-310-100) in 4˚C on rotation. Post-incubation, beads were then washed and the HIS-tagged proteins were eluted with lysis buffer supplemented with 250 mM Imidazole. Samples for gel electrophoresis analysis were collected throughout the purification to confirm pull down and elution of the protein of interest via Coomassie staining. Protein was subsequently buffer-exchanged and concentrated for injection onto GE HiTrap Ion Exchange Q or SP column on an AKTA Pure. Final samples were concentrated to approximately ~10mg/mL before flash freezing and storage.

Mutagenesis

Gatekeeper mutations were made using overlapping primers via site-directed mutagenesis. Following PCR amplification and DpnI digestion of nascent methylated

plasmid, bacterial transformation yielded colonies that were picked and sequenced to confirm the desired nucleotide/codon changes.

Differential Scanning Fluorimetry

5 µM of purified p38 protein were incubated in the presence of vehicle (DMSO) or varying concentrations of compounds in 25 mM Tris, 150 mM NaCl, 20 mM $MgCl_2$. After a 10-minute incubation, Sypro-Orange Protein Cell Stain 5000X (Thermo Fisher Item # S6650) was added to the protein mixture to a final 10X concentration. Protein melting temperatures were determined by a ROX readout on QuantStudio 5 Real-Time PCR machine, with 1˚C per minute increases from 25 to 99˚C. The derivative of the melting curves was obtained using Protein Thermal Shift Software 1.3. Temperatures at the peaks of maximum fluorescence were determined using GraphPad Prism software and melting temperature was also plotted.

Hierarchical Clustering

To generate hierarchical clustering heat maps of the *in vitro* kinase inhibition profiles, the inhibition data was organized via Python 3.6 packages: seaborn, pandas, and matplotlib. Pandas was used to load the data frame. Both seaborn and matplotlib were used to cluster (average method), visualize, adjust sizing, and label accordingly.

RNA Extraction and Sequencing of HCC Cell Lines

HUH7 and THLE5B cells were plated in 6-well plates, treated for 24 hrs with 0.1% DMSO, 5 µM sorafenib, or 50 nM AD80. Cellular RNA was extracted using the RNeasy mini kit (Qiagen) the same day following manufacturer's instructions. RNA quality was calculated by the RNA Integrity Number (RIN) as provided by 2100 Bioanalyzer. RNA-seq was conducted on poly-A enriched RNA, 175 bp single reads using an Illumina HiSeq2500 instrument. Libraries were constructed using the TruSeq Stranded mRNA Library Prep Kit using the standard protocol. Raw sequencing reads were mapped to the GRCh37/hg19 reference genome (UCSC) using STAR (2.4.0c)(20). Aligned reads were mapped to GRCh37/hg19 genetic features. Counts had a median coverage of 33.6 million

mapped reads per sample. Quality control was performed using RSeQC and Picard, including unsupervised clustering **(Supp Fig. 2)**(21).

Functional Analysis of HCC Cell Line RNA Sequencing

The DeSeq2 package for R was used to calculate differentially expressed genes between the 3 treatment conditions using a generalized linear model(22). Gene set enrichment analysis (GSEA)(23) was used to determine if any Hallmark or KEGG gene sets were significantly enriched among the differentially expressed genes between each of the 3 conditions, respectively (FDR <.05)(24). Enrichment scores were determined from a running sum statistic when the statistic is at the maximum deviation from zero.

Compounds and Chemical Syntheses

Skepinone-L was purchased from SelleckChem (S7214). The AD compounds, sorafenib, and regorafenib were synthesized as previously described; details are provided in the supplemental synthetic methods section. Final compounds were characterized by NMR on a 400 MHz Bruker Avance III HD system and a Xevo TQD UPLC-mass spectrometer (Waters).

AD80 Signature and Survival Analysis on TCGA

To generate the AD80 gene signature we used the differentially expressed genes between HUH7 cells treated with AD80 and DMSO. Specifically, we selected those genes with log2 fold change higher or lower than 3 (FDR<0.05). We used normalized FPKM expression values from the patients within the TCGA-LIHC dataset(25). In total, we included 359 HCC patients in the analysis, for whom clinical annotation data were also available. We used the Nearest Template Prediction(26) method to identify those patients with a tumor expression profile enriched in genes of the AD80 signature, following the same approach as previously reported(27). We evaluated the prognostic impact of the signature with log-rank test and used Kaplan-Meier curves for representation of overall survival in patients with and without the signature as implemented in the Survminer package and plotted in Graphpad Prism. Comparison of AFP levels between patients with and without the signature was done using the Wilcoxon rank-sum test. All analyses were

conducted using R 3.3.3. RNA-seq has been deposited at Array Express under accession number E-MTAB-7847.

We also used the TCGA-LIHC(25) data for p38 survival analyses. Data on 365 patients were stratified based on how significantly different the expression of each isoform was to determine expression cutoffs. We evaluated the prognostic impact as done above in patients with and without the AD80 signature.

Rescue Experiments

Plasmids: pCDNA3-Flag MKK6$^{S207E,\ T211E}$ (#13517) and pCDNA3-Flag p38 gamma (#20353) plasmids were created by Roger Davis and obtained through Addgene (Watertown, MA). Mutant primers for p38 gamma^{M109T} were obtained from Integrated DNA Technologies (Coralville, IA). The pCDNA3-Flag p38 gamma^{M109T} plasmid was generated following the QuikChange II site-directed mutagenesis protocol by Agilent (Santa Clara, CA). After transformation of the plasmid into One Shot^{TM} Stbl3^{TM} chemically competent cells (Invitrogen, Carlsbad, CA), DNA was isolated using Qiagen® Plasmid Midiprep Kit (Qiagen, Hilden, Germany) and the mutant DNA sequence was confirmed by Sanger sequencing (Genewiz, South Plainfield, NJ).

Transfection: HUH7 and HEP3B cells were transfected with MKK6$^{S207E,\ T211E}$, p38 gamma, and p38 gamma^{M109T} plasmids following the Lipofectamine^{TM} 3000 protocol (Invitrogen, Carlsbad, CA). For growth inhibition assays, 5 x 10^4 cells were plated per well in a 96-well dish with 0.2 µg DNA per well. For western blotting, 1 x 10^6 cells were plated per well in a 6-well dish with 5 µg DNA per well.

Growth inhibition assays: HUH7 and HEP3B cells were treated with either DMSO or AD80 (1 µM, 0.5 µM, 0.1 µM, or 0.05 µM) 24 hours after transfection. After 96 hours of treatment, resazurin sodium salt (Sigma-Aldrich, St. Louis, MO) was added to each well for a final concentration of 0.01 µg/µl, and fluorescence was measured using a spectrophotometer after a two-hour incubation. Technical triplicates for each condition were averaged and normalized percent cell viability was determined by dividing the average fluorescence for sample wells by DMSO-treated wells for each respective condition and multiplying by

100. Percent growth inhibition was determined by normalizing inhibitor-treated samples to DMSO controls.

Western Blotting: Treated cells were harvested, washed with PBS, and lysed in RIPA Buffer (Thermo Fisher Scientific, Waltham, MA) for 30 minutes on ice. Lysates were centrifuged at 14,000G at 4° C for 10 minutes and the protein concentration of the supernatant was determined by DC™ protein assay (Bio-Rad, Hercules, CA). Equal amounts of total protein (60 – 80 μg) were resolved by SDS-PAGE and transferred onto PVDF membranes. Blots were probed overnight at 4° C with antibody raised against the protein of interest. Anti-FLAG® M2 antibody was obtained from Sigma-Aldrich and used at a 1:10,000 dilution. Phospho-ATF2 (Thr71) antibody was obtained from Invitrogen and used at a 1:500 dilution. Vinculin (E1E9V) XP® antibody was obtained from Cell Signaling Technology and used at a 1:1000 dilution. GAPDH antibody was obtained from Abcam and used at a 1:10000 dilution. After incubation with peroxidase-conjugated secondary antibodies, proteins were detected using chemiluminescence.

Statistical Analysis

Data are expressed as mean±SD. Statistical significance was determined using Mann-Whitney U test (when n <10 or non-normal distribution) or Student's t-test (n >10 and normal distribution). Correlation was calculated using the Pearson test. Group size was determined based on the results of preliminary experiments and using the "resource equation" method, where "E" - the degree of freedom of analysis of variance - should be a value between 10 and 20. For the mouse experiment, "E" was the total number of animals minus the total number of groups. Group allocation was performed randomly while outcome assessment was not performed in a blinded manner. The differences in survival were plotted using Kaplan-Meier curves. Significance was determined using Log-rank (Mantel-Cox) test and the Gehan-Breslow-Wilcoxon test. GraphPad Software was used to create the graphs and for the statistical analysis. Significance values were set at *p<0.05, **p<0.01, ***p<0.001, and ****p<0.0001.

RESULTS:

A type II kinase inhibitor screen identifies AD80 as a highly potent compound in experimental models of HCC

A major focus of our research group concerns the identification of chemical probes and lead compounds for therapeutic development(28,29). As part of our efforts we have focused on the synthesis of small molecule modulators of kinase signaling networks and protein complex assembly. This library of chemical probes, which now includes several hundred in-house synthesized type II KIs, was screened against a panel of five different HCC cell lines including HUH7, PLC/PRF/5, Hep3B, Li-7, and SNU398. We included several series of compounds with variations at the hinge binding, linker, and cap motifs synonymous with type II inhibition (**Fig. 1A**), some of which were previously published(28,30). Our preliminary analysis included growth inhibition assays on several HCC cell lines and an SV40 immortalized adult hepatocyte line THLE5B, with sorafenib and regorafenib – each displaying 50% growth inhibition (GI_{50}) concentrations ranging from 5-20 μM on these lines - included as controls (**Fig. 2A-F**). Through this analysis, we identified the compound AD80 as ranging from 10 to 1000-fold more potent than either sorafenib or regorafenib (**Fig. 2A-F**). HUH7, a well-differentiated hepatocyte-derived cellular carcinoma cell line, and HEP3B, a hepatoma line, were especially sensitive to AD80 with GI_{50} values of 35.6 ± 21 nM, and 7.1 ± 1 nM, respectively (**Fig. 2G**). THLE5B, which acts as control for effects on non-transformed liver tissue, had a markedly higher GI_{50} for AD80 at 2.84 ± 0.81 μM. These initial studies suggested AD80 as a potent lead compound relative to sorafenib or regorafenib.

To further evaluate AD80, we conducted long-term clonogenic assays to measure effects on replicative capacity (**Fig. 2G**). These clonogenic assays further revealed AD80 as at least 100-fold more potent on HCC cell lines compared to sorafenib (**Fig. 2G**). However, at doses that caused growth inhibition on HUH7 lines, AD80 had no measurable effects on THLE5B. In contrast, sorafenib was equally or slightly more potent on THLE5B compared to HUH7. Indeed, growth inhibition assays indicated a larger therapeutic window for AD80 compared to sorafenib (**Fig. 2H**). Overall, the growth inhibition and clonogenic assays suggested selectivity for tumor over normal cells for AD80 as

compared to sorafenib, regorafenib, and several drugs that have been tested in HCC clinical trials(31).

AD80 is highly active in a tumor xenograft model

To further explore the anti-tumoral activity of AD80, we generated HUH7 xenografts in athymic nude *Foxa1/nu* mice (**Fig. 3A**). Experimental dosing for AD80 (20 mg/kg) was determined from maximum tolerated dosage (MTD) studies and pharmacokinetic (PK) analysis (**Supp. Fig. 1**). In agreement with our cell line assays, AD80 demonstrated significantly improved activity relative to sorafenib, extending the time before each xenograft reached 1000 mm^3, which was the humane endpoint (maximum survival 31 days). Overall survival, compared to both vehicle (maximum survival of 13 days) and sorafenib (maximum survival of 19 days) was also improved with AD80 (**Fig.3A**). AD80 also significantly reduced the tumor growth rate per day compared to vehicle and sorafenib (**Fig. 3B**), with rates reduced by half in AD80 versus vehicle treated animals: 32.3 ± 9.9 %/day versus 57.1 ± 7.5 %/day, respectively. There was also a 31.8% reduction in tumor growth rate comparing AD80 to sorafenib: 32.3 ± 9.9 %/day versus 47.4 ± 7.3 %/day, respectively.

We harvested tumors from each animal following final dosing for western blot analysis of the mitogen-activated protein kinase (MAPK) and mammalian target of rapamycin (mTor) pathways; proposed biomarkers of sorafenib efficacy(32,33). Intriguingly, the animals that survived the longest in the sorafenib and AD80 arms displayed relatively weak phospho-ERK1/2(Thr202/Tyr204) signals compared to controls (**Fig. 3C-D**). In contrast, inhibition of phospho-RPS6(Ser235/236) was not associated with differences in survival. This result is consistent with previous work suggesting that the efficacy of sorafenib in HCC models depends on inhibition of ERK signaling(34,35). Similarly, the activity of AD80 in this model may also occur, at least in part, through inhibition of MAPK/ERK signaling.

AD80 induces transcriptomic reprograming to a less aggressive phenotype in cell lines and human samples

To delineate the transcriptomic changes induced by AD80 relative to sorafenib, we performed RNA-sequencing on HUH7 cells treated for 24 hours with either DMSO, sorafenib, or AD80. Using principal component analysis, we found a clear discrimination between treatment groups (**Supp. Fig. 2**), which suggests that AD80 and sorafenib induce highly divergent transcriptomic perturbations in HUH7 cells. 8,416 and 9,590 genes were significantly deregulated between AD80 and sorafenib compared to DMSO, respectively (FDR <0.01). Compared to either the DMSO control or sorafenib treatment AD80 induced a marked up-regulation in numerous genes associate with normal hepatocyte physiology, including many involved in metabolic pathways, suggesting modulation of HUH7 towards a normal hepatocyte state in response to this compound (**Fig. 4A**). Members of the MAPK family, including MAPK1 (ERK2), MAP3K7 (TAK1), and MAPK13 (p38delta), were significantly down-regulated in AD80 treatment compared to sorafenib. Further, sorafenib treatment paradoxically increased expression of several MAPK signaling proteins, such as RAS family members. To evaluate AD80 on normal hepatocytes, we treated THLE5B cells with the same conditions as described for HUH7. Overall, there were notably much fewer genes deregulated by AD80 in the THLE5B hepatocyte cell line than in HUH7. Specifically, the expression of metabolic and MAPK signaling genes significantly altered by AD80 in HUH7 were unchanged in THLE5B cells (**Fig. 4A**). Thus, the greater therapeutic window of AD80 versus sorafenib likely stems from two features: first, an induction of HUH7 cells to a normal hepatocyte-like state as reflected by the changes in metabolic genes, and secondly, through pronounced down-regulation of MAPK family members.

We further performed gene set enrichment analysis (GSEA) using the ranked gene expression differences between AD80, sorafenib, and DMSO for both KEGG (**Supp. Fig. 3**) and the Broad Institute Hallmark gene-sets(24) (**Fig. 4B**). Common between sorafenib and AD80 were many downregulated gene sets involved in oncogenesis, such as epithelial to mesenchymal transition genes, angiogenesis, MYC and E2F targets. Several of these gene sets were also downregulated in THLE5B cells by AD80 and sorafenib treatment, albeit to a lesser degree, with normalized enrichment scores for MYC and E2F targets 2 to 3-fold lower. Notably, these oncogenic targets are largely downstream of MAPK signaling(36). Further, in almost all cases, there was a stronger down-regulation

of oncogenic pathways by AD80 compared to sorafenib even though a dose equivalent to GI_{50} was used for both inhibitors.

We also found marked differences between AD80 and sorafenib on metabolic gene sets including xenobiotic metabolism, bile acid metabolism, and cholesterol metabolism; all significantly up-regulated by AD80 but not by sorafenib (**Fig. 4B**). We next generated a gene signature associated to AD80 exposure in HUH7 cells (**Supp. Table 1)**. We hypothesized that patients with a gene expression profile resembling the one induced by AD80 would have a better clinical profile. Using the Nearest Template Prediction method(26), we identified 18% (65/359) of patients with a tumor expression profile significantly enriched (FDR<0.05) in our AD80 signature. These patients had significantly better survival compared to those patients lacking the AD80 signature (P=0.008, **Fig. 4C)**. As predicted, those patients with the AD80 signature had significantly lower levels of AFP (P<0.001), a known poor prognostic marker in HCC (**Fig. 4D**). In summary, the RNA sequencing data suggests AD80 could be reprograming HCC transcriptome towards a less aggressive tumor phenotype by up-regulating liver and metabolism specific genes, while also reducing oncogenic signaling; both of these effects markedly distinguish AD80 from sorafenib.

p38 delta (MAPK12) and gamma (MAPK13) as direct targets of AD80

AD80 was originally developed as a polypharmacological kinase inhibitor of RET-mutant tumors(28). However, RET is neither mutated or expressed in the cancer cell lines used in our study based on published data(37,38). More recently, AD80 has been demonstrated as highly active in lung cancer models containing Kif5B-Ret fusions(39) and also in PTEN-deficient malignancies(40). Our study is the first to demonstrate high activity of AD80 in liver cancer models.

To identify critical targets for AD80 specific to HCC, we conducted an unbiased proteomic screen. All expressed and active kinases in HUH7 cells were labeled with the activity-based probe ATP-desthiobiotin (ATP^{bio})(19) in the presence or absence of 1 μM of AD80, with the degree of ATP^{bio}-inhibition by AD80 measured through quantitative mass spectrometry on labeled peptides (**Fig. 5**). We found over 250 kinases within HUH7 cell lysates that were both expressed and labeled by the ATP-desthiobiotin probe;

labeling on 20 of these kinases was inhibited by greater than 60% in the presence of AD80 (Fig. 5, **Supp Table 2)**. RET was not detected in these experiments using mass spectrometry, which supports the lack of RET expression and activity in this cell line. The top inhibited kinases included several tyrosine kinases (EPHA2, FAK, EPHB4, ABL2, LYN), cell-division kinases (AURKA, AURKB, and AURKC), members of the stress activated p38 family (p38δ and p38γ), and several additional mitogen-activated protein kinases (GCK, KHS1, and TAK1).

Due to the wide number of putative kinase targets, we used correlative structure-activity relationships (SAR) to identify critical targets of AD80 within HUH7. For this, we tested a small number of AD80-analogs, including the AD80-related compound AD58 (**Fig. 6A**). Interestingly, AD58 was 100-fold less active in the HUH7 cell line compared to AD80 (**Fig. 6B**). However, based on in vitro assays, AD58 targeted many of the overlapping kinases that are inhibited most strongly by AD80 within HUH7 cells(28). This overlap in activity for AD80 and AD58 on the Aurora kinases, FRK, LYN, KHS, ABL2, and GCK, suggests these kinases as unlikely critical targets for the differential activity of AD80 versus AD58 in this cell line. Consistent with this idea, although AD80 has activity on Aurora A, we did not find any indication of MYC degradation **(Supp. Fig. 4),** which has previously been suggested as a marker of Aurora A inhibition within HCC cell lines[23]. The most critical target that differentiated AD80 from AD58, and from the additional compounds AD57 and AD81, based on the HCC profiling and in vitro activity, included EPHA2, EPHB4 and p38γ, with the strongest correlation mapped to p38γ (**Fig. 6C**). This data supports potentially important roles for all of these kinases within HUH7. However, based on the SAR, and the transcriptional effects on MAPK signaling genes, we further evaluated the possible isoform-biased activity among p38 family members by AD80. Notably, unlike AD80, the majority of known p38 inhibitors display isoform biased activity towards p38 alpha and beta.

To test the isoform selectivity of AD80 on the p38s, each human isoform was expressed and purified to homogeneity for biochemical analysis (**Supp. Fig. 5**). Differential scanning fluorimetry (DSF) was used to test binding of AD80 and several control compounds. In this assay, binding is measured as a change in protein melting temperature due to ligand-induced stabilization(41). AD80 was compared to DMSO or a

known p38 alpha inhibitor skepinone-L(42). Skepinone-L specifically increased the melting temperature of p38 alpha (ΔT_m=13.87˚C) and p38 beta (ΔT_m=9.88˚C) (**Fig. 6D**). Sorafenib also demonstrated biased binding for the p38 alpha and beta forms (ΔT_m=7.44 and 7.19˚C, respectively). AD58 had little to no binding for any isoform. Conversely, AD80 demonstrated selectivity toward p38 gamma and delta, with ΔT_m=7.98˚C and ΔT_m=8.93 ˚C, compared to the ΔT_m=4.03˚C and ΔT_m=3.33 ˚C on p38 alpha and beta, respectively (**Fig. 6D**). The activity on p38 delta in our assay was not observed in the large-scale in vitro profiling presented in **Fig. 6C;** we account for this difference based on variances in protein purifications and assays. However, the activity of AD80 on both p38 gamma and delta agrees with the close homology in these two isoforms. Overall, based on the binding data, we suggest that AD80 represents a novel kinase inhibitor for p38 gamma and delta biased polypharmacology.

One notable difference between p38 family members is the residues at the gatekeeper positions **(Supp. Fig. 6).** Alpha and beta both have a small threonine at position 106, while gamma and delta both have the larger methionine at positions 109 and 107, respectively. To test the influence of the gatekeeper residue, point mutations were made in each isoform and again tested using our biochemical melting temperature assay **(Supp. Fig. 5, Fig. 6E)**. In contrast to wild-type p38s, AD80 bound more favorably towards alpha and beta isoforms over delta and gamma, with ΔT_m=12.14 and 9.91˚C for alpha^{T106M} and beta^{T106M}, respectively, versus ΔT_m=3.88 and 4.77˚C for gamma^{M109T} and delta^{M107T}, respectively (**Fig. 6E).** This data supports that the gatekeeper residue largely controls AD80 selectivity among p38 members, and that AD80-binding is active site-directed with a rare preference for methionine over threonine at the gatekeeper.

To test for rescue from AD80 inhibition, we over-expressed wild-type p38γ, the gatekeeper mutant M109T, and an activated form of the upstream p38 kinase MKK6$^{S207E, T211E}$ in HUH7 and HEP3B cells. These lines were chosen as they represent the two most sensitive HCC cell lines to AD80 growth inhibition (**Fig. 2**), and MKK6$^{S207E, T211E}$ was included as it serves as an upstream activating kinase for all four p38 isoforms (**Supp. Fig. 7A**,(43)). In HEP3B, each construct provided a statistically significant reduction in AD80 growth inhibition based on area under the curve (AUC) comparisons ($p<0.001$ for both MKK6$^{S207E, T211E}$ and WT p38γ, and $p=0.0065$ for p38γ^{M109T}; **Supp. Fig. 7B**). In

contrast, only MKK6$^{S207E,\ T211E}$ significantly reduced AD80 activity in HUH7 cells (p=0.0056), suggesting that the rescue may occur independently of p38 gamma in this line. Western blot analysis downstream of MKK6 and p38 members on the transcription factor substrate ATF2 found relatively higher pATF2 signals in the presence of AD80 compared to controls that appeared to correlate with rescue from AD80 growth inhibition (**Supp. Fig. 7C**). Overall, the growth inhibition and western blot data supports the hypothesis that rescue from AD80 growth inhibition occurs through sustained MKK6➔p38➔ATF2 signaling. However, distinct activated p38 isoform(s) downstream of MKK6$^{S207E,\ T211E}$ can likely drive resistance to AD80 in different cell lines.

Low expression of p38 delta and gamma in human HCC correlates with favorable survival

The SAR analysis of AD80 and related analogs, combined with mass spectrometry and *in vitro* profiling, suggests p38 gamma and delta as key dependencies in several HCC cell lines. Whereas the rescue experiments indicate that sustained MKK6➔p38➔ATF2 signaling can drive resistance to AD80. To further evaluate the potential role of p38 delta and gamma as correlates of aggressive HCC, we evaluated their prognostic impact in the TCGA liver cancer dataset, which includes 365 patient samples(25). Low and high expression groups for each of the p38 isoforms were plotted against survival. Low mRNA expression levels of p38 gamma and delta showed a statistically favorable prognosis for survival over high expression groups (**Fig. 7A-B**). This difference was specific to the gamma and delta isoforms over alpha and beta (**Fig. 7C-D**). This data supports that inhibition of p38 gamma and delta, especially within high expression individuals, may be useful as an adjunct for existing treatments to prolong survival for HCC patients.

Discussion:

In this study we discover novel targets and companion inhibitors for HCC. We utilize a focused library of structurally related kinase inhibitors with conformational selectivity for the type II DFG-out conformation. At the outset, we hypothesized that the use of such a compound library across multiple pre-clinical models of HCC may uncover target kinases that may be invisible to more conventional reverse genetic screens using tools such as RNAi or CRISPR; with the difference being loss of protein versus exploitation of a specific conformational state of a target. Through this approach we identified p38 gamma and delta as promising targets for HCC, and the compound AD80 as a type II inhibitor biased towards these members of the p38 family.

HCC has proven an extremely difficult to treat cancer, with most therapeutic advances generated through the use of multi-targeted KIs. Recently, immune checkpoint antibodies such as Nivolumab have demonstrated response rates as high as ~15% for HCC patients(44). While this response rate is in line with what has been observed in other cancers, a substantial number of patients do not respond. This points to the need for discovering both new biochemical and mechanistic targets for HCC, as well as new lead compounds for this disease that can be applied to broad groups of patients. Using a small molecule library, we were able to identify AD80 as a compound with nearly a 100-fold higher activity on HCC cell lines compared to some of the lead FDA-approved small molecule inhibitors. Further, AD80 was also able to reduce tumor growth in a xenograft model of liver cancer. This occurred coincident with the ability of AD80 to inhibit key driver signaling pathways (e.g. ERK) pertinent to liver cancer, as well as induce up-regulation of liver-specific genes that are important for normal liver function and survival. We also discovered that AD80 was able to inhibit several kinases where low expression has been correlated to improved overall survival for HCC patients. In this regard, we focused on p38 gamma and delta kinases due to compelling correlative structure-activity-relationship and HCC survival analysis.

The p38 family of kinases has been described as a stress-responsive family of proteins that are stimulated by various signals including cytokines and free fatty acid (FFA) accumulation(45). The family has partially overlapping roles with the JNK1-3 kinases, with members activated by MAP2K kinases MKK 3, 4, 6, and 7(46). The critical

substrates of the p38 kinases include transcription factors such as c-JUN(47), ELK1(48), and ATF2(49). Intriguingly, despite similar signaling and biochemistry, previous studies have suggested marked differences between the biology of the different p38 isoforms. For example, the alpha isoform is required for growth and development, and p38 alpha deficient mice show embryonic lethality; whereas, p38 beta, gamma, and delta knockouts are all viable(50,51). The alpha isoform is ubiquitously expressed, whereas again, the other 3 isoforms have much more restricted expression patterns. Notably, most studies with p38 inhibitors have focused on compounds such as skepinone-L and SB-203580, which are heavily alpha-biased and likely limited due to p38α-related toxicity. Indeed, a phase I trial of the p38 alpha inhibitor LY3007113 failed due to unacceptable toxicity(52). In contrast, p38 gamma and delta double-knockouts are viable, and these mice have been used to demonstrate specific inflammatory roles for these kinases within macrophages, T-cells, and myeloid cells(53,54). These studies point to biomarkers and cell-types for further analysis with p38 gamma and delta biased-inhibitors such as AD80. They also provide potential insights on the whole-animal tolerability from inhibition of p38 gamma and delta.

The preference of AD80 for p38 kinases with bulkier gatekeeper residues (Met in gamma and delta versus Thr in alpha and beta) is quite unusual. Other type II kinase inhibitors, such as imatinib and sorafenib, have a strong preference for Thr over larger residues. Indeed, a highly common drug resistant mutant of imatinib is the T315I mutation in BCR-ABL(55). While our in vitro binding assays using M➔T mutations suggests an inverted preference for larger residues at the gatekeeper by AD80, our rescue experiments did not markedly separate the wild-type and M109T mutant of p38γ. This potentially indicates that resistance to AD80 is unlikely to develop through single point mutations at the gatekeeper residue of p38 gamma or delta, and therefore other mechanisms of resistance to this compound should be investigated. For example, studies in another well-established AD80 target, RET, have found non-gatekeeper drug resistance mutations(39). Additionally, our ‘rescue’ experiment suggests another possible mechanism for resistance through sustained p38➔ATF2 signaling via activated MKK6. A future area of investigation will be to determine if type II inhibitors that bind strongly to all four p38 isoforms can be generated, and if so, will such compounds be well tolerated.

AD80 represents a promising lead upon which to examine this question through additional analog development. Further optimization of AD80's physiochemical properties for clinical development, including solubility, are also warranted. As are identifying predictive biomarkers - for example, possibly p38 gamma or delta expression - as patient selection criteria for this therapeutic approach.

Since MKK6 is known to activate all four isoforms of p38 (**Supp. Fig. 7A**), we interpret the stronger rescue from AD80 by activated MKK6$^{S207E/T211E}$, but less significant rescue with an individual p38 isoform, as possibly resulting from combinations of p38 activity, including potentially p38 alpha and beta. Notably, resistance to sorafenib via p38 alpha and activation of ATF2 has been described previously(15), providing more support for the importance of p38 signaling in HCC drug resistance. Our current experiments cannot distinguish which isoforms drive rescue that arises from over-expression of MKK6, and we have left this as an area of future investigation. Other future experiments will focus on the mechanism through which AD80 drives the significant up-regulation in liver function genes, some of which - ALDH family up-regulation, for example - have been linked to recurrence free survival(56). A better understanding of this biology could guide tailoring of the compound to further enhance its promise for HCC. Experiments are also underway to understand how p38 gamma and delta modulate the liver cancer microenvironment. Taken together, AD80 represents a lead compound upon which to build a drug that both inhibits oncogenic signaling, while promoting normal liver function.

Acknowledgements

This research was supported by NIH grants NCI F31CA210639 (J.X. Yu), T32CA078207 (A.J. Craig), T32GM062754 (M.E. Duffy), and RO1CA227636 (A.C. Dar) as well as awards from Damon Runyon-Rachleff Foundation DRR28-15 (A.C. Dar), and Tisch Cancer Institute P30 CA196521, along with seed funds from a Tisch Cancer Institute Development Funding Award (A.C. Dar., A. Lujambio, A. Villanueva). A.C. Dar is a Pew-Stewart Scholar in Cancer Research and Young Investigator of the Pershing-Square Sohn Cancer Research Alliance. A. Villanueva is supported by the U.S. Department of Defense (CA150272P3). A. Lujambio is supported by the U.S. Department of Defense (CA150272P2 and CA150178) and the Damon Runyon-Rachleff Foundation (DR52-18). V. Miguela was supported by the U.S. Department of Defense (CA150272P2 and CA150178). M. Ruiz de Galarreta was supported by Fundación Alfonso Martín Escudero Fellowship and Damon Runyon-Rachleff Innovation Award (DR52-18).

REFERENCES

1. Bray F, Ferlay J, Soerjomataram I, Siegel RL, Torre LA, Jemal A. Global cancer statistics 2018: GLOBOCAN estimates of incidence and mortality worldwide for 36 cancers in 185 countries. CA Cancer J Clin. 2018;68:394–424.

2. Villanueva A. Hepatocellular Carcinoma. N Engl J Med. 2019;380:1450–62.

3. AACR Cancer Progress Report Writing Committee, Sawyers CL, Abate-Shen C, Anderson KC, Barker A, Baselga J, et al. AACR Cancer Progress Report 2013. Clin Cancer Res Off J Am Assoc Cancer Res. 2013;19:S4-98.

4. Cleary SP, Jeck WR, Zhao X, Chen K, Selitsky SR, Savich GL, et al. Identification of driver genes in hepatocellular carcinoma by exome sequencing. Hepatol Baltim Md. 2013;58:1693–702.

5. Fujimoto A, Totoki Y, Abe T, Boroevich KA, Hosoda F, Nguyen HH, et al. Whole-genome sequencing of liver cancers identifies etiological influences on mutation patterns and recurrent mutations in chromatin regulators. Nat Genet. 2012;44:760–4.

6. Schulze K, Imbeaud S, Letouzé E, Alexandrov LB, Calderaro J, Rebouissou S, et al. Exome sequencing of hepatocellular carcinomas identifies new mutational signatures and potential therapeutic targets. Nat Genet. 2015;47:505–11.

7. Ling S, Hu Z, Yang Z, Yang F, Li Y, Lin P, et al. Extremely high genetic diversity in a single tumor points to prevalence of non-Darwinian cell evolution. Proc Natl Acad Sci U S A. 2015;112:E6496-6505.

8. Zehir A, Benayed R, Shah RH, Syed A, Middha S, Kim HR, et al. Mutational landscape of metastatic cancer revealed from prospective clinical sequencing of 10,000 patients. Nat Med. 2017;23:703–13.

9. Cheng A-L, Kang Y-K, Lin D-Y, Park J-W, Kudo M, Qin S, et al. Sunitinib versus sorafenib in advanced hepatocellular cancer: results of a randomized phase III trial. J Clin Oncol Off J Am Soc Clin Oncol. 2013;31:4067–75.

10. Llovet JM, Ricci S, Mazzaferro V, Hilgard P, Gane E, Blanc J-F, et al. Sorafenib in advanced hepatocellular carcinoma. N Engl J Med. 2008;359:378–390.

11. Kudo M, Finn RS, Qin S, Han K-H, Ikeda K, Piscaglia F, et al. Lenvatinib versus sorafenib in first-line treatment of patients with unresectable hepatocellular carcinoma: a randomised phase 3 non-inferiority trial. The Lancet. 2018;391:1163–73.

12. Abou-Alfa GK, Meyer T, Cheng A-L, El-Khoueiry AB, Rimassa L, Ryoo B-Y, et al. Cabozantinib (C) versus placebo (P) in patients (pts) with advanced hepatocellular carcinoma (HCC) who have received prior sorafenib: Results from the randomized phase III CELESTIAL trial. J Clin Oncol. 2018;36:207–207.

13. Bruix J, Qin S, Merle P, Granito A, Huang Y-H, Bodoky G, et al. Regorafenib for patients with hepatocellular carcinoma who progressed on sorafenib treatment (RESORCE): a randomised, double-blind, placebo-controlled, phase 3 trial. The Lancet. 2017;389:56–66.

14. Adnane L, Trail PA, Taylor I, Wilhelm SM. Sorafenib (BAY 43-9006, Nexavar), a dual-action inhibitor that targets RAF/MEK/ERK pathway in tumor cells and tyrosine kinases VEGFR/PDGFR in tumor vasculature. Methods Enzymol. 2006;407:597–612.

15. Rudalska R, Dauch D, Longerich T, McJunkin K, Wuestefeld T, Kang T-W, et al. In vivo RNAi screening identifies a mechanism of sorafenib resistance in liver cancer. Nat Med. 2014;20:1138–46.

16. Dauch D, Rudalska R, Cossa G, Nault J-C, Kang T-W, Wuestefeld T, et al. A MYC-aurora kinase A protein complex represents an actionable drug target in p53-altered liver cancer. Nat Med. 2016;22:744–53.

17. Okamoto K, Ikemori-Kawada M, Jestel A, von König K, Funahashi Y, Matsushima T, et al. Distinct binding mode of multikinase inhibitor lenvatinib revealed by biochemical characterization. ACS Med Chem Lett. 2015;6:89–94.

18. Wilhelm SM, Dumas J, Adnane L, Lynch M, Carter CA, Schütz G, et al. Regorafenib (BAY 73-4506): a new oral multikinase inhibitor of angiogenic, stromal and oncogenic receptor tyrosine kinases with potent preclinical antitumor activity. Int J Cancer. 2011;129:245–55.

19. Patricelli MP, Nomanbhoy TK, Wu J, Brown H, Zhou D, Zhang J, et al. In Situ Kinase Profiling Reveals Functionally Relevant Properties of Native Kinases. Chem Biol. 2011;18:699–710.

20. Dobin A, Davis CA, Schlesinger F, Drenkow J, Zaleski C, Jha S, et al. STAR: ultrafast universal RNA-seq aligner. Bioinformatics. 2013;29:15–21.

21. Wang L, Wang S, Li W. RSeQC: quality control of RNA-seq experiments. Bioinforma Oxf Engl. 2012;28:2184–5.

22. Love MI, Huber W, Anders S. Moderated estimation of fold change and dispersion for RNA-seq data with DESeq2. Genome Biol. 2014;15:550.

23. Subramanian A, Tamayo P, Mootha VK, Mukherjee S, Ebert BL, Gillette MA, et al. Gene set enrichment analysis: a knowledge-based approach for interpreting genome-wide expression profiles. Proc Natl Acad Sci U S A. 2005;102:15545–50.

24. Liberzon A, Birger C, Thorvaldsdóttir H, Ghandi M, Mesirov JP, Tamayo P. The Molecular Signatures Database Hallmark Gene Set Collection. Cell Syst. 2015;1:417–25.

25. Comprehensive and Integrative Genomic Characterization of Hepatocellular Carcinoma. Cell. 2017;169:1327-1341.e23.

26. Hoshida Y. Nearest Template Prediction: A Single-Sample-Based Flexible Class Prediction with Confidence Assessment. PLOS ONE. 2010;5:e15543.

27. Villanueva A, Hoshida Y, Battiston C, Tovar V, Sia D, Alsinet C, et al. Combining clinical, pathology, and gene expression data to predict recurrence of hepatocellular carcinoma. Gastroenterology. 2011;140:1501-1512.e2.

28. Dar AC, Das TK, Shokat KM, Cagan RL. Chemical genetic discovery of targets and anti-targets for cancer polypharmacology. Nature. 2012;486:80–4.

29. Dhawan NS, Scopton AP, Dar AC. Small molecule stabilization of the KSR inactive state antagonizes oncogenic Ras signalling. Nature. 2016;537:112–6.

30. Sonoshita M, Scopton AP, Ung PMU, Murray MA, Silber L, Maldonado AY, et al. A whole-animal platform to advance a clinical kinase inhibitor into new disease space. Nat Chem Biol. 2018;14:291–8.

31. Scudellari M. Drug development: Try and try again. Nature. 2014;516:S4–6.

32. Masuda M, Chen W-Y, Miyanaga A, Nakamura Y, Kawasaki K, Sakuma T, et al. Alternative Mammalian Target of Rapamycin (mTOR) Signal Activation in Sorafenib-resistant Hepatocellular Carcinoma Cells Revealed by Array-based Pathway Profiling. Mol Cell Proteomics MCP. 2014;13:1429–38.

33. Calvisi DF, Ladu S, Gorden A, Farina M, Conner EA, Lee J-S, et al. Ubiquitous activation of Ras and Jak/Stat pathways in human HCC. Gastroenterology. 2006;130:1117–28.

34. Liu L a b, Cao Y a, Chen C a, Zhang X a, McNabola A a, Wilkie D a, et al. Sorafenib blocks the RAF/MEK/ERK pathway, inhibits tumor angiogenesis, and induces tumor cell apoptosis in hepatocellular carcinoma model PLC/PRF/5. Cancer Res. 2006;66:11851–8.

35. Zhang Z, Zhou X, Shen H, Wang D, Wang Y. Phosphorylated ERK is a potential predictor of sensitivity to sorafenib when treating hepatocellular carcinoma: evidence from an in vitro study. BMC Med. 2009;7:41.

36. Gramling MW, Eischen CM. Suppression of Ras/Mapk pathway signaling inhibits Myc-induced lymphomagenesis. Cell Death Differ. 2012;19:1220–7.

37. Barretina J, Caponigro G, Stransky N, Venkatesan K, Margolin AA, Kim S, et al. The Cancer Cell Line Encyclopedia enables predictive modeling of anticancer drug sensitivity. Nature. 2012;483:603–7.

38. Pharmacogenomic agreement between two cancer cell line data sets | Nature [Internet]. [cited 2018 Mar 8]. Available from: https://www.nature.com/articles/nature15736

39. Plenker D, Riedel M, Brägelmann J, Dammert MA, Chauhan R, Knowles PP, et al. Drugging the catalytically inactive state of RET kinase in RET-rearranged tumors. Sci Transl Med. 2017;9.

40. Liu H, Feng X, Ennis KN, Behrmann CA, Sarma P, Jiang TT, et al. Pharmacologic Targeting of S6K1 in PTEN-Deficient Neoplasia. Cell Rep. 2017;18:2088–95.

41. Vollrath F, Hawkins N, Porter D, Holland C, Boulet-Audet M. Differential Scanning Fluorimetry provides high throughput data on silk protein transitions. Sci Rep. 2014;4:5625.

42. Koeberle SC, Romir J, Fischer S, Koeberle A, Schattel V, Albrecht W, et al. Skepinone-L is a selective p38 mitogen-activated protein kinase inhibitor. Nat Chem Biol. 2012;8:141–3.

43. Enslen H, Brancho DM, Davis RJ. Molecular determinants that mediate selective activation of p38 MAP kinase isoforms. EMBO J. 2000;19:1301–11.

44. El-Khoueiry AB, Sangro B, Yau T, Crocenzi TS, Kudo M, Hsu C, et al. Nivolumab in patients with advanced hepatocellular carcinoma (CheckMate 040): an open-label, non-comparative, phase 1/2 dose escalation and expansion trial. The Lancet. 2017;389:2492–502.

45. Cargnello M, Roux PP. Activation and function of the MAPKs and their substrates, the MAPK-activated protein kinases. Microbiol Mol Biol Rev MMBR. 2011;75:50–83.

46. Manieri E, Sabio G. Stress kinases in the modulation of metabolism and energy balance. J Mol Endocrinol. 2015;55:R11-22.

47. Willaime-Morawek S, Brami-Cherrier K, Mariani J, Caboche J, Brugg B. C-Jun N-terminal kinases/c-Jun and p38 pathways cooperate in ceramide-induced neuronal apoptosis. Neuroscience. 2003;119:387–97.

48. Patel M, Predescu D, Tandon R, Bardita C, Pogoriler J, Bhorade S, et al. A novel p38 mitogen-activated protein kinase/Elk-1 transcription factor-dependent molecular mechanism underlying abnormal endothelial cell proliferation in plexogenic pulmonary arterial hypertension. J Biol Chem. 2013;288:25701–16.

49. Breitwieser W, Lyons S, Flenniken AM, Ashton G, Bruder G, Willington M, et al. Feedback regulation of p38 activity via ATF2 is essential for survival of embryonic liver cells. Genes Dev. 2007;21:2069–82.

50. Beardmore VA, Hinton HJ, Eftychi C, Apostolaki M, Armaka M, Darragh J, et al. Generation and characterization of p38beta (MAPK11) gene-targeted mice. Mol Cell Biol. 2005;25:10454–64.

51. Sabio G, Arthur JSC, Kuma Y, Peggie M, Carr J, Murray-Tait V, et al. p38gamma regulates the localisation of SAP97 in the cytoskeleton by modulating its interaction with GKAP. EMBO J. 2005;24:1134–45.

52. Goldman JW, Rosen LS, Tolcher AW, Papadopoulos K, Beeram M, Shi P, et al. Phase 1 and pharmacokinetic study of LY3007113, a p38 MAPK inhibitor, in patients with advanced cancer. Invest New Drugs. 2017;

53. Risco A, del Fresno C, Mambol A, Alsina-Beauchamp D, MacKenzie KF, Yang H-T, et al. p38γ and p38δ kinases regulate the Toll-like receptor 4 (TLR4)-induced cytokine production by controlling ERK1/2 protein kinase pathway activation. Proc Natl Acad Sci U S A. 2012;109:11200–5.

54. González-Terán B, Matesanz N, Nikolic I, Verdugo MA, Sreeramkumar V, Hernández-Cosido L, et al. p38γ and p38δ reprogram liver metabolism by modulating neutrophil infiltration. EMBO J. 2016;35:536–52.

55. Gorre ME, Mohammed M, Ellwood K, Hsu N, Paquette R, Rao PN, et al. Clinical resistance to STI-571 cancer therapy caused by BCR-ABL gene mutation or amplification. Science. 2001;293:876–80.

56. Suzuki E, Chiba T, Zen Y, Miyagi S, Tada M, Kanai F, et al. Aldehyde dehydrogenase 1 is associated with recurrence-free survival but not stem cell-like properties in hepatocellular carcinoma. Hepatol Res Off J Jpn Soc Hepatol. 2012;42:1100–11.

FIGURE LEGENDS

Figure 1: Clinical kinase inhibitors for HCC share common structural features that enable conformation specific binding. A. Sorafenib and regorafenib are both approved for first-line and second-line treatment of HCC; their chemical structures differ by a single fluorine. Cabozantinib and lenvatinib are also promising therapies for HCC. All four compounds share several conserved structural motifs: the hinge-binding element functions as an adenosine mimic, the linker and cap extend deep into the kinase active site pocket. B. Top: Phosphorylated insulin receptor tyrosine kinase in complex with peptide substrate and ATP analog within an active state DFG (aspartate-phenylalanine-glycine)-IN configuration (PDB ID: 1IR3), where the ATP analog is able to interact with the DFG loop, and thus amenable to both substrate recognition and phosphorylation (Bottom). C. Top: Binding of sorafenib to BRAF (PDB ID: 1UWH) forces the kinase to adopt the DFG-OUT conformation. In this state, the BRAF activation-segment (A-seg; bottom) adopts an inactive conformation. The DFG-OUT form of binding is referred to as Type II inhibition.

Figure 2: The Type II inhibitor AD80 is highly active across multiple in vitro models of HCC. A-F. HCC and hepatocyte cell lines incubated with 0.3 nM to 20 μM of AD80, Sorafenib, and Regorafenib in 0.1% DMSO (n≥3 technical). G. Calculated GI_{50} values of drugs from A-F on cell lines (mean±SD in μM). H. Clonogenic crystal violet assay of THLE5B, immortalized hepatocyte cell line, and HUH7, treated under the indicated conditions for 14 days. Each condition was tested in triplicate. I. Therapeutic window calculated based on normalization of GI_{50} values from normal (THLE5B) and transformed (HUH7) lines for the indicated compounds.

Figure 3: AD80 significantly improves survival in a pre-clinical HCC model through enhanced inhibition of the ERK/MAPK pathway. A. Mouse survival in a HUH7 xenograft model. B. AD80 treated animals show a tumor growth rate that is half of vehicle treated animals, and significantly less than sorafenib treated animals. C. Western blot analysis of individual tumors harvested from animals at the end of the survival experiment shown in D. Note that mice that survived longest in D displayed relatively weak phospho-ERK1/2 signal compared to mice that died early. Antibodies used: S6 Ribosomal Protein(S6RP) (5G10), phospho-S6 Ribosomal Protein(S6RP) (Ser235/236, Phospho-p44/42 MAPK (Erk1/2) (Thr202/Tyr204), p44/42 MAPK (Erk1/2) (137F5). Blots were run in duplicate; representative data is shown.

Figure 4: AD80 induces an increased metabolism and reduced oncogenic signaling gene signature compared to sorafenib in HUH7 cells. The AD80-induced gene signature

significantly correlates to greater overall survival and lower AFP levels based on TCGA-LIHC data set. A. Heat map of metabolism and MAPK associated genes significantly upregulated or downregulated across the three groups within the indicated cell lines. Color key denotes the Z-Score (number of standard deviations from the mean) of the sample and gene row. B. Gene set enrichment analysis based on HUH7 data against the Hallmark Gene Sets, where normalized enrichment scores (NES) are shown as bars and false discovery rate (FDR) < 0.05 is marked by an asterisk. For A and B, three biological replicates per treatment near the IC_{50} dose (sorafenib 5 µM, AD80 50 nM, DMSO 0.1%) on HUH7 or THLE5B cell lines as indicated, over a course of 24 hours, were completed. C. Kaplan-Meier survival comparison of TCGA-LIHC patient samples, separated by patients with (+) or without (-) the genes upregulated/downregulated by AD80 (Supplemental Table 3). Log-rank (Mantel-Cox) testing used to determine significance. Summary of number of patients at risk every 2.5 years, separated based on AD80 signature shown below the Kaplan-Meier. D. Box and whisker plot of TCGA-LIHC AD80 signature.

Figure 5: Activity-based protein profiling by mass spectrometry identifies kinases strongly inhibited by AD80 in the HUH7 cell line. % inhibition (y-axis) corresponds to the difference in kinase labeling with ATP-desthiobiotin in AD80 treated samples compared to untreated controls for each kinase shown along the x-axis. AD80-treated and untreated samples were analyzed in duplicate and quadruplicate, respectively. See supplementary Table 2 for raw profiling data.

Figure 6: AD80 is isoform biased for p38γ and p38δ, over p38α and p38β, with binding dependent on the gatekeeper residue. A. Chemical structure of AD80 and related compounds. B. Cell viability assay comparing activity of each compound on the HUH7 cell line. Technical replicates n=6. C. Hierarchical clustering of previously generated in vitro inhibitory profiles (ref. *(28)*) of the most different kinases between the related compounds. D-E. Melting temperature binding assay using a 1:1 ratio of drug to protein (ie. 5 µM drug to 5 µM protein). Each point is the difference in mean melting temperature (technical replicates: n=6) as determined by differential scanning fluorimetry. In E the following mutations at the gatekeeper residue were tested: p38α/MAPK14 T106M, p38β/MAPK11 T106M, p38γ/MAPK12 M109T, p38δ/MAPK13 M107T.

Figure 7: Low mRNA expression of p38γ and p38δ correlates with significantly better overall survival for individuals with liver cancer. A-D. Kaplan-Meier overall survival curves for individuals with low (blue) and high (red) p38 isoform expression based on liver cancer TCGA data compiled from the Protein Atlas. Expression cutoffs between high versus low were 0.7 Fragments Per Kilobase of transcript per Million mapped reads (FPKM) (MAPK12), 0.2 FPKM

(MAPK13), 9.6 FPKM (MAPK14), and 2.7 FPKM (MAPK11). In all panels, p-values were determined using log-rank (Mantel-Cox) testing.

Author Manuscript Published OnlineFirst on June 18, 2019; DOI: 10.1158/1535-7163.MCT-18-0571
Author manuscripts have been peer reviewed and accepted for publication but have not yet been edited.

Figure 1

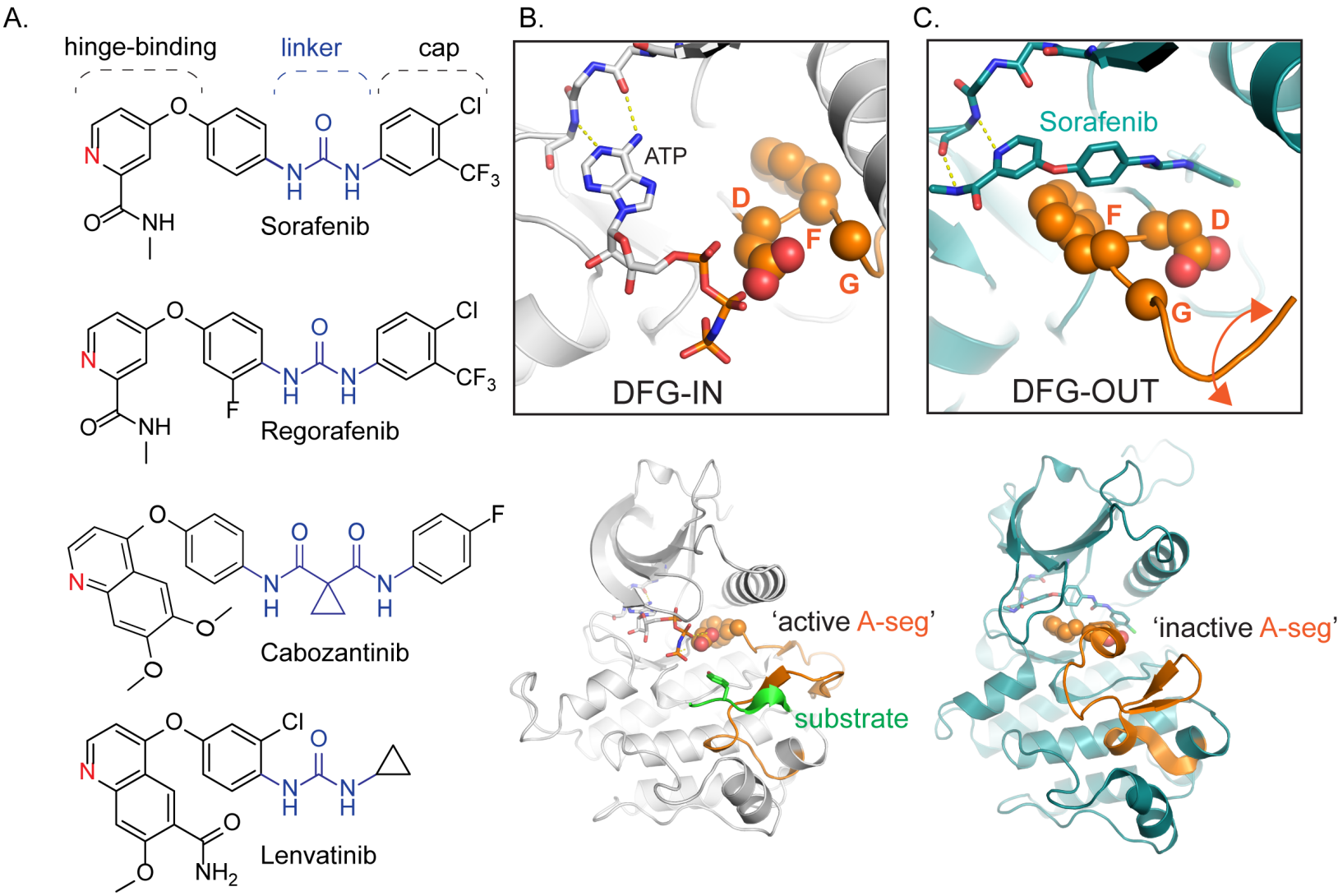

Author Manuscript Published OnlineFirst on June 18, 2019; DOI: 10.1158/1535-7163.MCT-18-0571
Author manuscripts have been peer reviewed and accepted for publication but have not yet been edited.

Figure 2

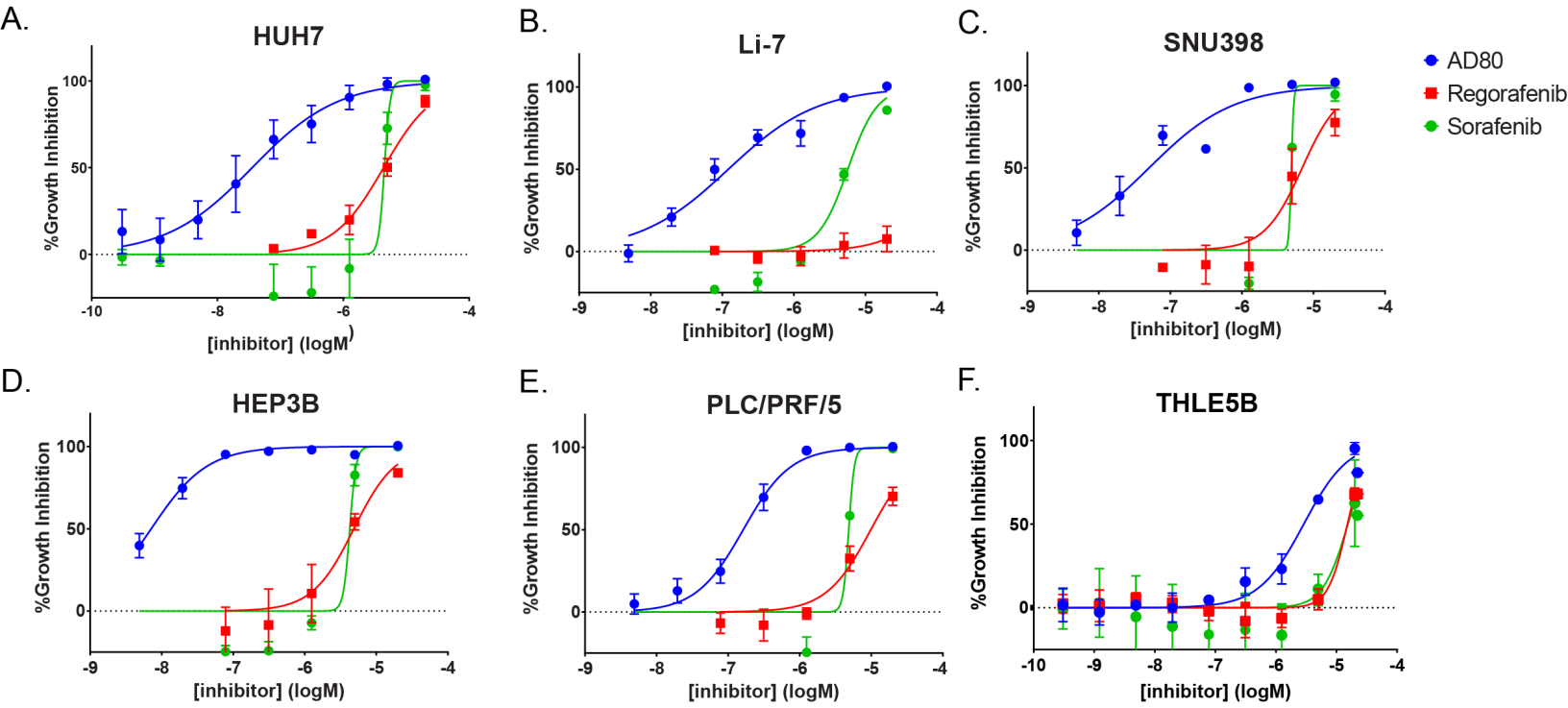

G.

GI50 (μM)	HUH7	LI7	SNU398	HEP3B	PLC/PRF/5	THLE5B
AD80	0.04 ± 0.02	0.12 ± 0.004	0.05 ± 0.015	0.007 ± 0.001	0.162 ± 0.053	2.84 ± 0.81
Regorafenib	4.4 ± 1.1	>20	6.9 ± 3.1	4.8 ± 1.0	9.8 ± 2.2	15.2 ± 1.83
Sorafenib	4.5 ± 0.9	5.7 ± 0.3	4.9 ± 0.1	4.2 ± 0.2	4.8 0.1	>20

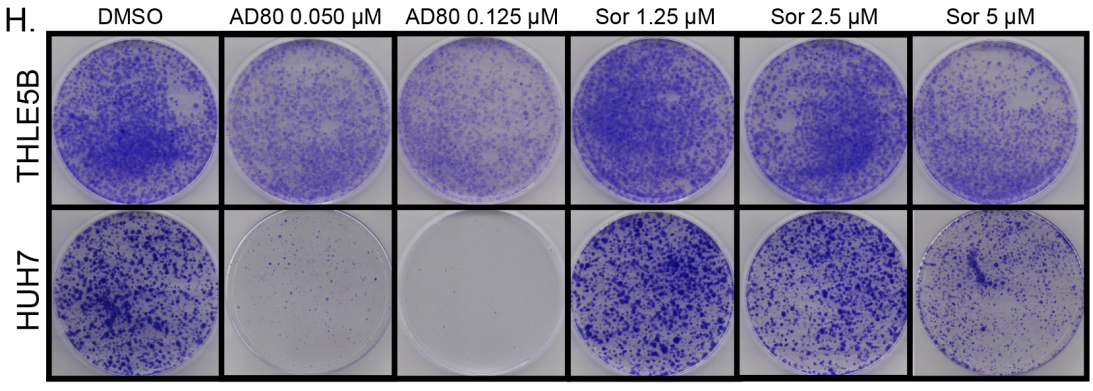

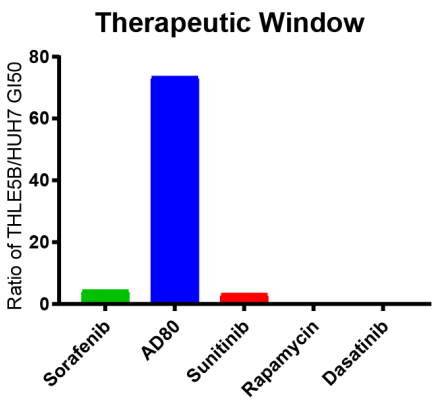

Author Manuscript Published OnlineFirst on June 18, 2019; DOI: 10.1158/1535-7163.MCT-18-0571
Author manuscripts have been peer reviewed and accepted for publication but have not yet been edited.

Figure 3

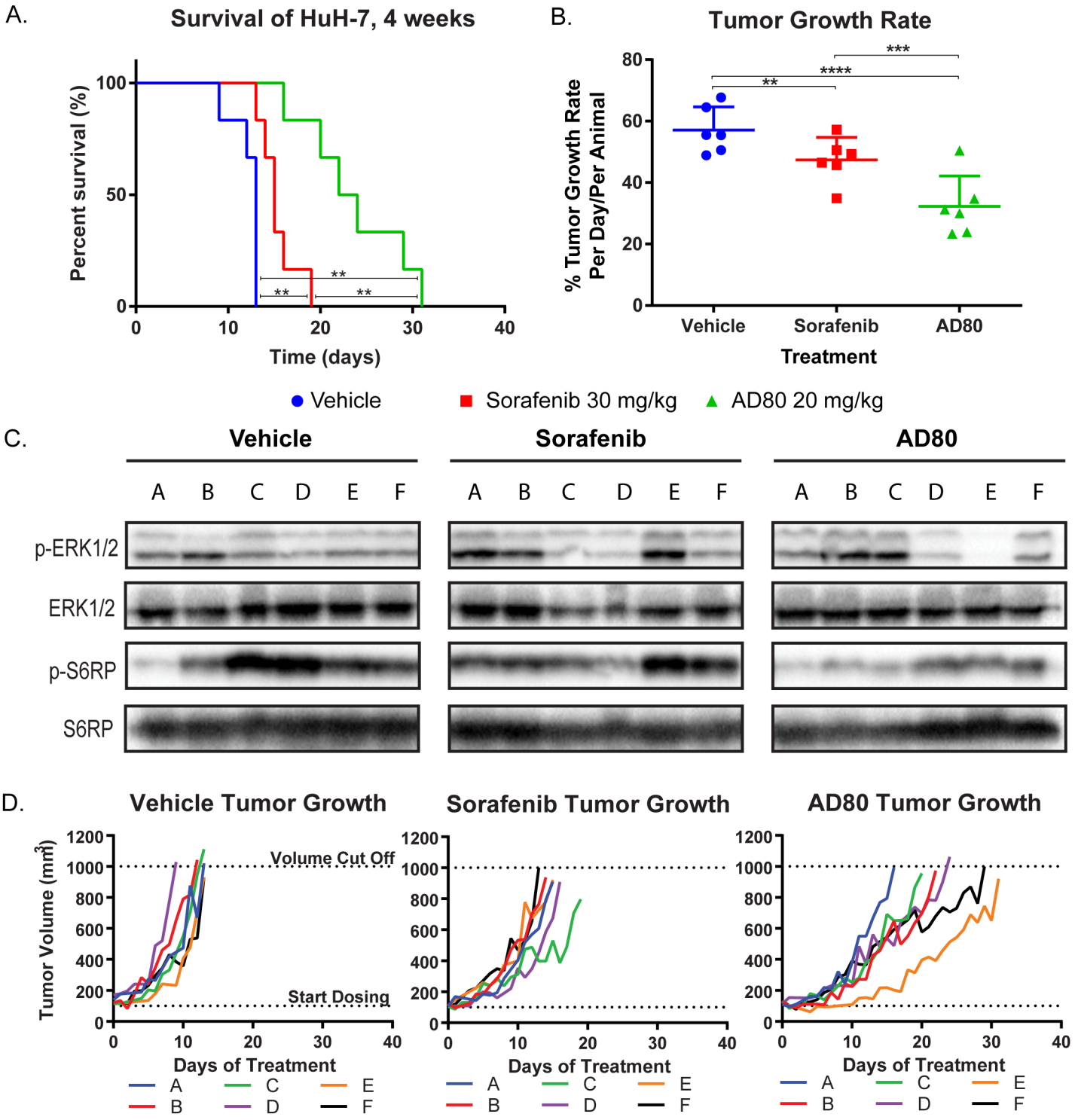

Figure 4 Author Manuscript Published OnlineFirst on June 18, 2019; DOI: 10.1158/1535-7163.MCT-18-0571
Author manuscripts have been peer reviewed and accepted for publication but have not yet been edited.

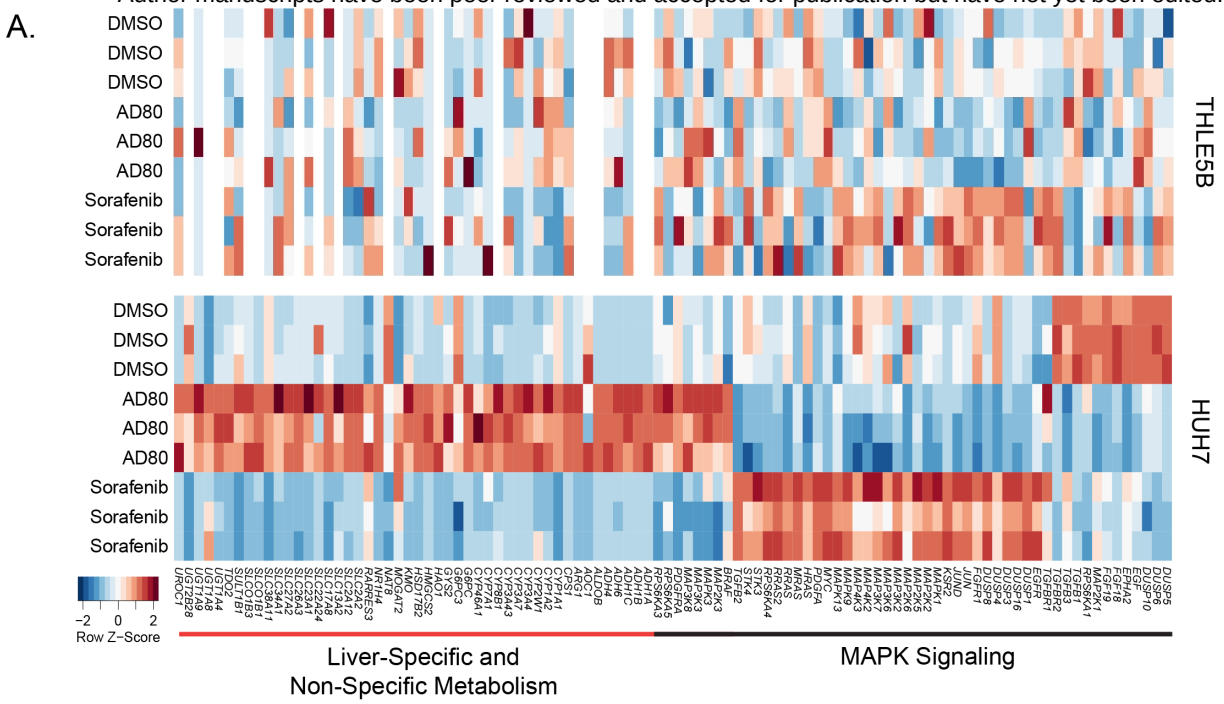

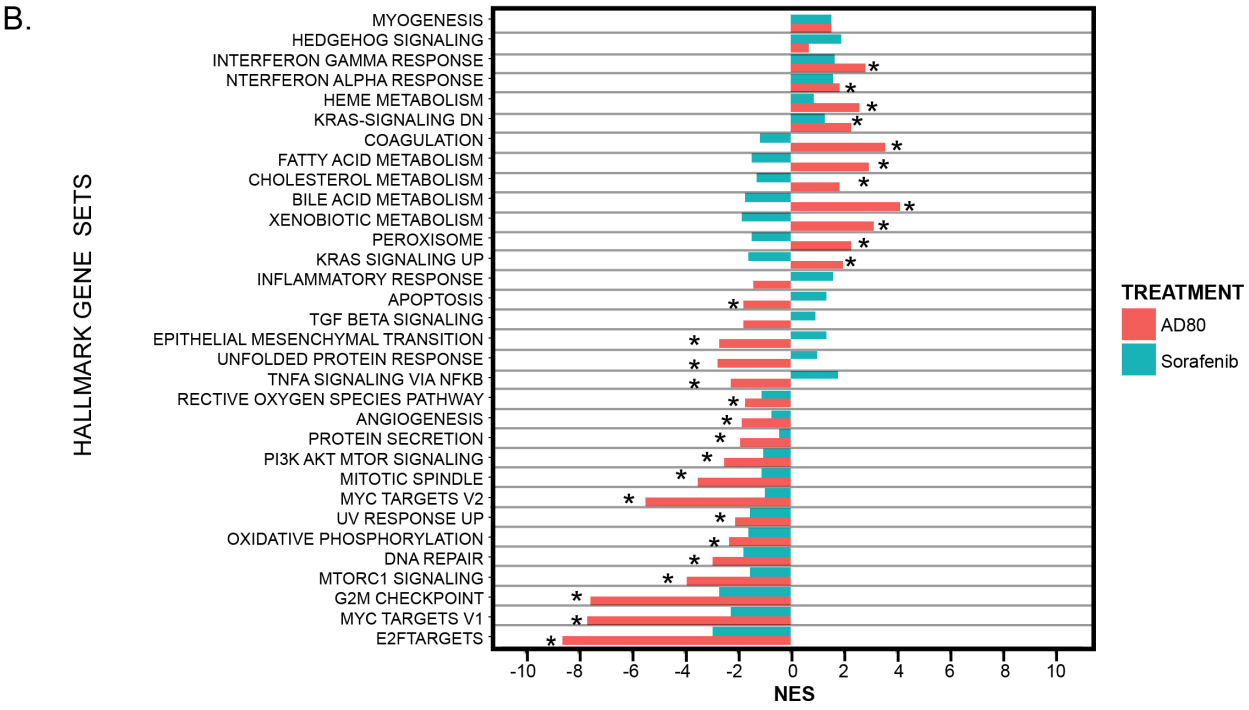

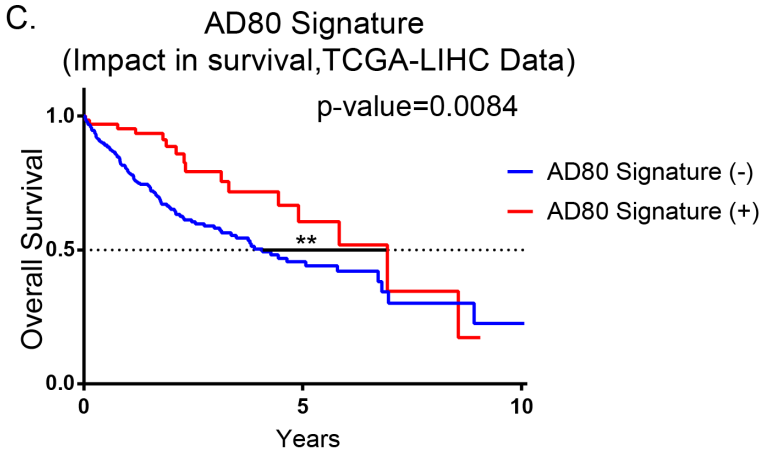

Number of Patients at Risk					
AD80 Signature (-)	294	82	30	6	1
AD80 Signature (+)	65	24	10	2	0
Years	0	2.5	5	7.5	10

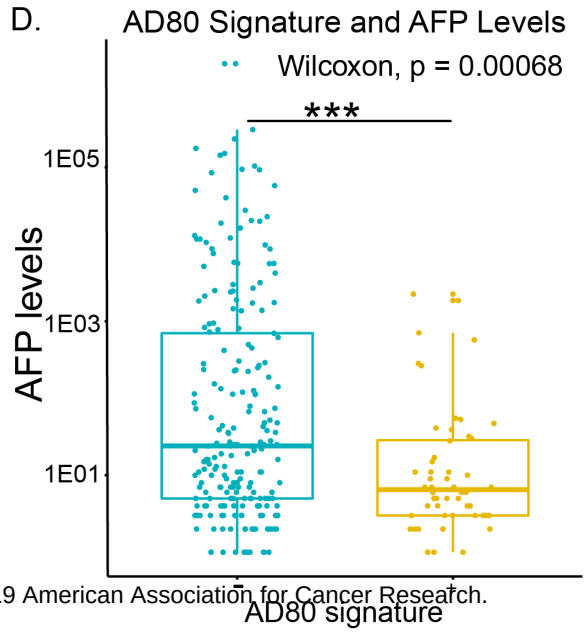

Author Manuscript Published OnlineFirst on June 18, 2019; DOI: 10.1158/1535-7163.MCT-18-0571
Author manuscripts have been peer reviewed and accepted for publication but have not yet been edited.

Figure 5

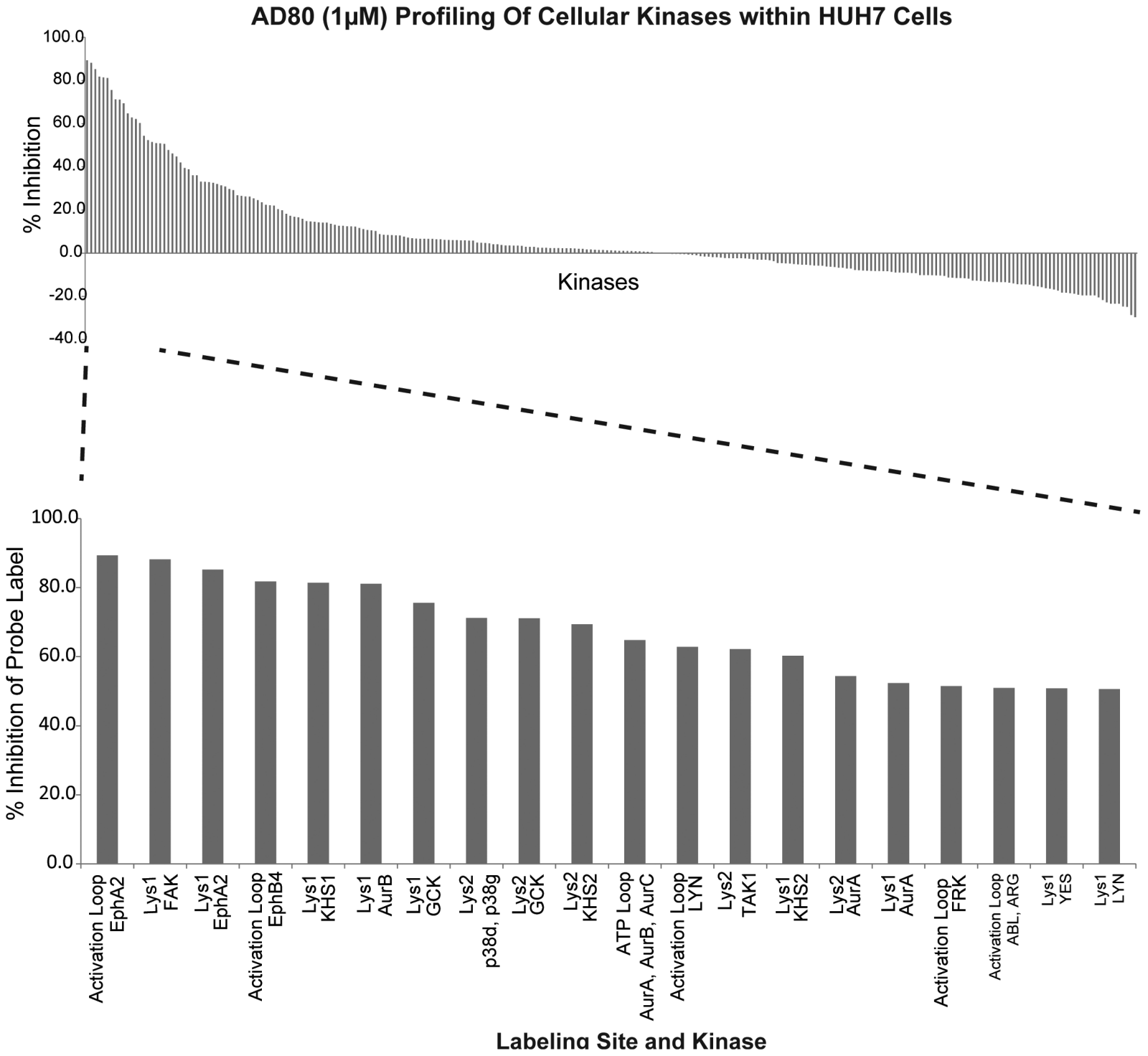

Author Manuscript Published OnlineFirst on June 18, 2019; DOI: 10.1158/1535-7163.MCT-18-0571
Author manuscripts have been peer reviewed and accepted for publication but have not yet been edited.

Figure 6

A.

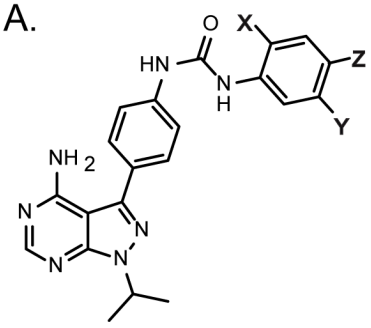

Name	X	Y	Z
AD80	F	CF_3	H
AD81	H	CF_3	Cl
AD57	H	CF_3	H
AD58	H	H	H

B.

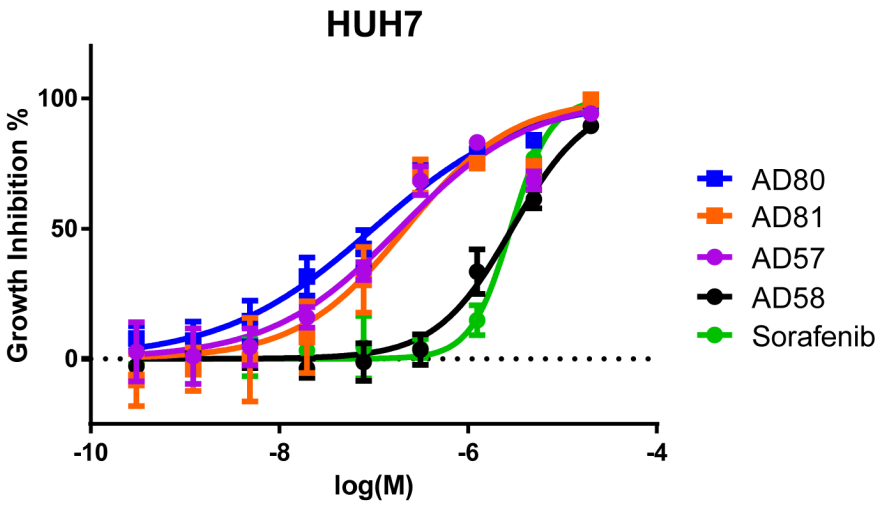

C.

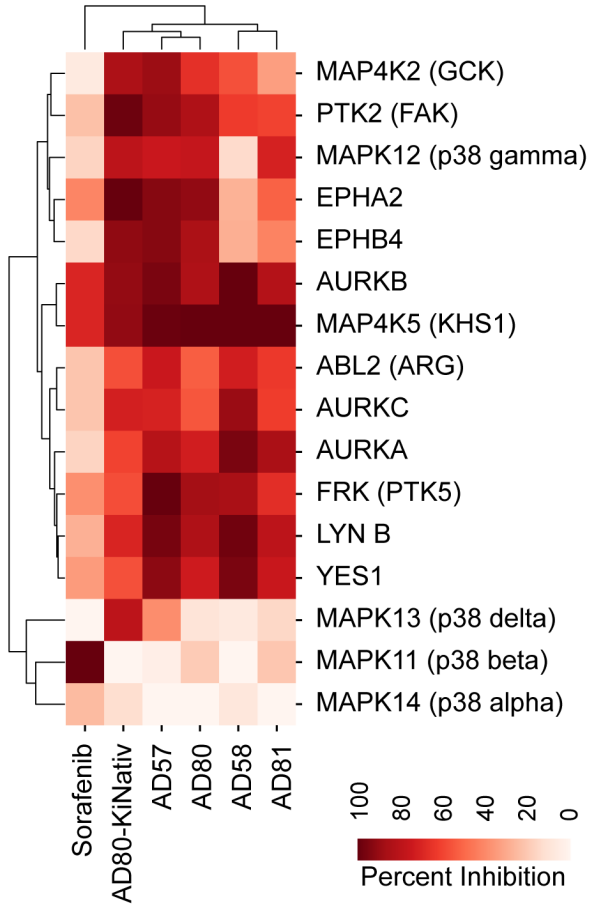

D.

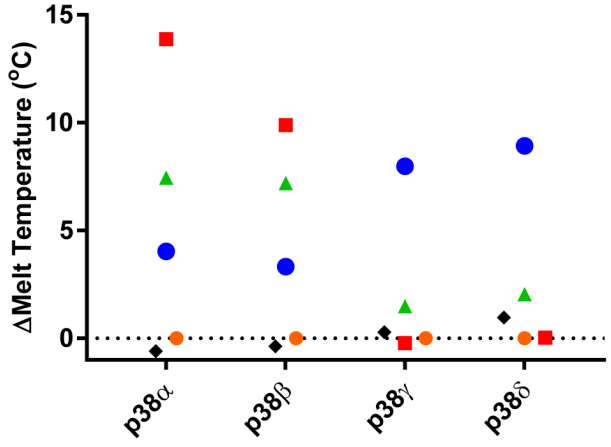

E.

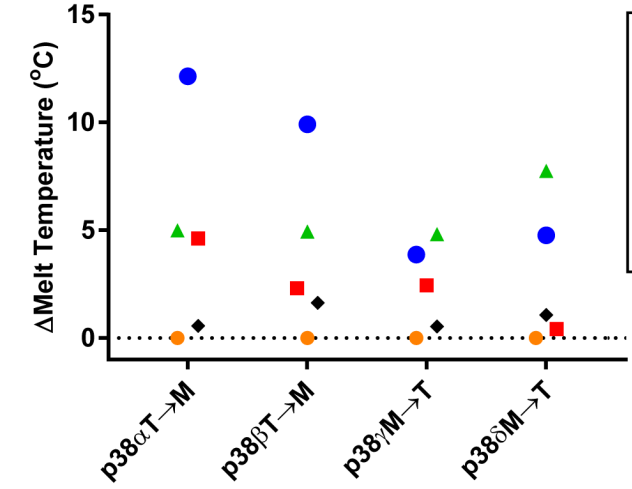

Author Manuscript Published OnlineFirst on June 18, 2019; DOI: 10.1158/1535-7163.MCT-18-0571
Author manuscripts have been peer reviewed and accepted for publication but have not yet been edited.

Figure 7

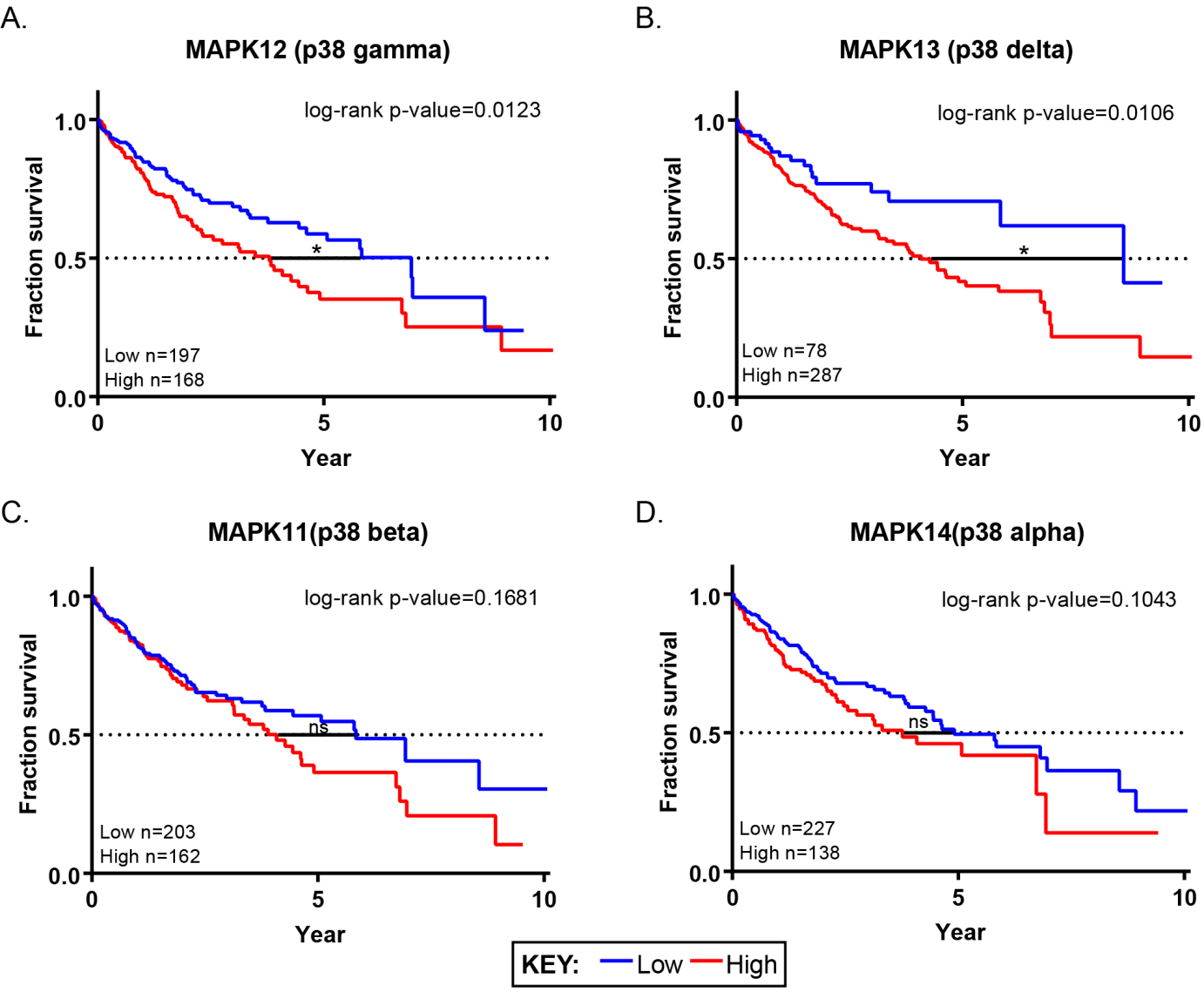

AACR American Association for Cancer Research

Molecular Cancer Therapeutics

Phenotype-based screens with conformation-specific inhibitors reveal p38 gamma and delta as targets for HCC polypharmacology

Jia Xin Yu, Amanda J Craig, Mary E Duffy, et al.

Mol Cancer Ther Published OnlineFirst June 18, 2019.